

Structural characterization of diamond-like carbon films for ultracold neutron applications

F. Atchison^a, T. Bryś^{a,d}, M. Daum^a, P. Fierlinger^{a,c,1}, A. Foelske^a, M. Gupta^{a,2}, R. Henneck^a, S. Heule^{a,c,*}, M. Kasprzak^{a,e}, K. Kirch^a, R. Kötz^a, M. Kuźniak^{a,f}, T. Lippert^a, C.-F. Meyer^b, F. Nolting^a, A. Pichlmaier^a, D. Schneider^b, B. Schultrich^b, P. Siemroth^b, U. Straumann^c

^a Paul Scherrer Institut, Villigen, Switzerland

^b Fraunhofer Institut für Werkstoff-und Strahltechnik, Dresden, Germany

^c Physik-Institut der Universität Zürich, Switzerland

^d Institut für Technische Chemie, ETH Zürich, Switzerland

^e Stefan Meyer Institut für subatomare Physik, Austrian Academy of Sciences, Vienna, Austria

^f Jagellonian University, Cracow, Poland

Received 2 September 2005; received in revised form 4 May 2006; accepted 28 June 2006

Available online 9 August 2006

Abstract

We have produced hydrogen-free diamond-like carbon (DLC) films by vacuum arc deposition for use as wall coating material in ultracold neutron (UCN) applications. The sp^3 fraction, the main quality factor for DLC used in UCN applications, was varied from 0.4 to 0.9, the coating thickness between 10 nm and 120 nm. The samples were characterized by using X-ray Absorption Near-Edge Spectroscopy (XANES), X-ray induced Photoelectron Spectroscopy (XPS), Laser induced surface Acoustic Waves (LAwave), cold neutron reflectometry and Raman spectroscopy at visible excitation wavelength. We observe reasonable agreement between the different results for film thicknesses below 20 nm. For larger thickness, we find that the surface-sensitive methods XPS and XANES yield smaller sp^3 fractions (by up to 20%) than the bulk-sensitive LAwave, being consistent with the assumption of a lower-density surface layer on a nominal-density bulk layer.

© 2006 Elsevier B.V. All rights reserved.

PACS: 78.70.Dm; 78.30.-j; 79.60.-i; 61.12.H; 81.15.Ef

Keywords: Diamond-like carbon; Characterization methods; sp^3 bonding; Laser arc deposition; Ultracold neutrons

1. Introduction

Diamond-like carbon (DLC), i.e. amorphous carbon with a significant sp^3 fraction, is nowadays used in various applications. In many of them, DLC not only replaces the original material but also brings improvements with it. This is also the case for our application, the use of hydrogen-free DLC as wall coating material for the transport and storage of ultracold neutrons (UCN).

Ultracold neutrons are free neutrons which are reflected on certain materials under any angle of incidence, their kinetic energy being less than the Fermi potential energy V [1] of the material. For suitable materials the Fermi potential can reach values up to about 300 neV, e.g. $V(\text{Be})=252$ neV or $V(^{58}\text{Ni})=346$ neV. They can thus be stored in material containers for times close to the neutron lifetime of about 15 min.

In the past, beryllium has been widely used as coating material for UCN storage applications, however as it is highly toxic, efforts are being made to replace it with the non-hazardous DLC [2–5]. The Fermi potential depends on the coherent scattering length of the material in question and on its mass density ρ . Thus, the development of improved DLC coatings has to go in the direction of high sp^3 fractions: the Fermi potential rises from 176 neV for zero porosity graphite ($\rho=2.25$ g/cm³) to 304 neV for pure diamond ($\rho=3.52$ g/cm³).

* Corresponding author. Paul Scherrer Institut, Villigen, Switzerland. Tel.: +41 56 310 3267; fax: +41 56 310 3120.

E-mail address: stefan.heule@psi.ch (S. Heule).

¹ Present address: Stanford University, MC: 4060, Varian 136, Stanford, California, 94305-4060, U.S.A.

² Present address: UGC-DAE Consortium for Scientific Research, Khandwa Road, Indore, IN-452 017, India.

The other important point for any UCN application is the reduction of the hydrogen content within the uppermost layer of about 10 nm thickness (i.e. the UCN penetration depth under reflection): UCN can easily gain enough kinetic energy from the hydrogen that they leave the UCN energy range, i.e. they are lost. The hydrogen reduction can be achieved by using clean vacuum coating methods, e.g. Pulsed Laser Deposition (PLD) or vacuum arc deposition. Also the contamination with elements of high neutron absorption cross section, like boron, has to be avoided, calling for high-purity graphite precursor material. For all these reasons hydrogen-free tetrahedral amorphous carbon (ta-C) is the DLC type of choice for UCN applications.

Promising results have been obtained recently for DLC coated foils prepared by laser induced vacuum arc deposition [6] in a new UCN storage experiment [4,5]. Vacuum arc deposition was also used to produce the samples described in this article.

As mentioned above, the ratio of sp^2 and sp^3 hybridized carbon atoms is the main quality parameter for DLC in UCN applications. We refer to the sp^3 fraction as the number of sp^3 hybridized carbon atoms divided by the total number of carbon atoms.

Characterization techniques for DLC are Electron Energy Loss Spectroscopy (EELS, see e.g. [7,8]), X-ray Photoelectron Spectroscopy (XPS, see e.g. [7,9]), Auger Electron Spectroscopy (AES, see e.g. [7]), X-ray Absorption Near-Edge Spectroscopy (XANES, see e.g. [10]), Raman Spectroscopy (see e.g. [11,12]), hardness measurements (see e.g. [13]) and Optical Ellipsometry (see e.g. [14]). Some of these methods are based on opto-electrical or mechanical properties while other methods exploit fundamental properties of the atomic structure like scattering of particles on the lattice. Therefore it is of principal interest for us to compare the results of some of them (Visible Raman Spectroscopy (Raman), XANES, XPS, Laser induced surface acoustic wave (LAwave)) with each other and with those of cold neutron reflectometry, which is closely related to the type of application we want to use the DLC for.

On a more practical level there is the demand for a well-tested technique which allows reliable measurement of the sp^3 fraction. Many studies, in particular those involving Raman Spectroscopy and XANES, have been used to establish a qualitative characterization of the sp^3 fraction, in order to decide whether one DLC film is more ‘diamond-like’ than another. Conducting a systematic comparison with different methods will allow to (a) derive calibration curves for methods which do not deliver absolute sp^3 fractions when used individually and (b) find a standard characterization procedure for DLC coatings used in UCN applications.

At the Paul Scherrer Institute we are implementing a facility to coat the insides of tubes by PLD at a laser wavelength of 193 nm. As part of the corresponding development program and in order to establish a fast and reliable characterization procedure (determination of the sp^3 fraction), we have conducted the comparative study presented here.

2. Samples

A series of eight DLC films with systematically varied sp^3 fraction was produced by physical vapour deposition (PVD),

Table 1
Process parameters and properties of the samples

Sample	Deposition method	Argon background press. [Pa]	Film thickness [nm]
1	Laser arc	0	105.0±0.1
2	Laser arc	0.06	117.6±0.2
3	Laser arc	0.17	118.7±0.2
4	Laser arc	0.33	105.3±0.2
5	Laser arc	0	12.0±0.1
6	Laser arc	0.06	11.3±0.1
7	High-current arc	–	45.0±0.8
8	High-current arc	–	17.0±0.4

using two slightly different deposition methods. The main part of the samples (films 1–6) was coated by unfiltered, laser controlled vacuum arc discharge [6]. Additional samples (films 7 and 8) were produced by magnetically filtered High-Current Arc deposition [15]. In order to get different film densities argon gas was added at different pressure levels: this affects the kinetic energy of the carbon species at deposition and thus the sp^3 fraction [16]. In order to test for effects which depend on the film thickness, films 5 and 6 were produced under identical conditions as films 1 and 2, but are much thinner. Different film thicknesses were achieved by using different deposition times. The film thickness was measured by ellipsometry (WVASE32 from Woollam Co.), see also [17]. Table 1 gives an overview of the process parameters and sample properties.

For all samples spectroscopically pure graphite (total impurity level less than 5 ppm) was used as target material. The films were deposited on standard silicon wafers, which, because of their smooth surfaces, allow production of thin films that still cover the whole surface. Because the different characterization methods required different sample sizes, the wafers were cut into pieces after deposition. The size of the pieces varied from a few mm^2 to about 4 cm^2 . The typical pressure before the addition of argon was less than $3 \cdot 10^{-3}$ Pa. The pulse length of the vacuum arc was about 100 μs , the current was 1300 A. The degree of ionization was close to 100% and ions had energies up to 50 eV. Our aim was to produce hydrogen-free DLC films with a thickness in the range of 100–300 nm, i.e. like samples 1 to 4. The thinner samples 5 to 8 were produced to cross-check the results from the thicker samples and to check the depth sensitivity of the different methods.

3. Characterization methods and results

The characterization methods used determine either the sp^2 fraction (XPS, XANES), the sp^3 fraction (XPS) or the density ρ (neutron reflectometry, LAwave) of the film. The relationship between the sp^3 fraction and the density of hydrogen-free amorphous carbon films was determined by Ferrari et al. with a linear fit of measured data and found to be [18]:

$$\rho \text{ (g/cm}^3\text{)} = 1.92 + 1.37 \cdot k, \quad (1)$$

where k is the sp^3 fraction. Assuming the amorphous structure to contain only sp^2 and sp^3 bonds, this equation can be derived from

$$\rho = (1-k) \cdot \rho_2 + k \cdot \rho_3 = \rho_2 + (\rho_3 - \rho_2) \cdot k \quad (2)$$

where ρ_3 and ρ_2 are the density of a totally sp^3 and a totally sp^2 bonded amorphous carbon film, respectively. The corresponding values for the densities are $\rho_3=3.29 \text{ g/cm}^3$ and $\rho_2=1.92 \text{ g/cm}^3$. Both values for an amorphous structure are well below those for the ordered structure (graphite up to 2.25 g/cm^3 , diamond 3.52 g/cm^3).

Since the Fermi potential (which is the relevant quantity for UCN applications) is calculated from the density ρ we convert the sp^2 and sp^3 fraction into density for the final comparison using Eqs. (1) and (2), respectively.

3.1. Raman spectroscopy

Raman spectroscopy can probe the structure of diamond-like carbon films. Depending on the excitation wavelength, the sp^2 or sp^3 bonds may be examined (sp^3 bonds only with UV-Raman). A detailed study of the Raman spectra of various types of amorphous carbon films taken at different excitation wavelengths can be found in [19]. For Raman studies with excitation light in the visible range, the contributions due to sp^2 sites dominate over those of sp^3 bonds, as e.g. investigated in [20].

The Raman spectrum of DLC shows a distinctive broad band with a maximum around 1580 cm^{-1} , as shown in Fig. 1 for sample 3. Standard deconvolution techniques resolve this into two bands, the Raman G band, which is centered around $1500\text{--}1600 \text{ cm}^{-1}$ and the Raman D band, which is centered around $1350\text{--}1400 \text{ cm}^{-1}$. For good-quality hydrogen-free DLC, the peak intensity (amplitude) ratio $I(D)/I(G)$ is found to be below 20% [11,19]. It has also been shown that the center position of the G band depends on the sp^3 fraction of the amorphous carbon film at short excitation wavelengths [19]. Internal stress in the amorphous carbon film may (also) cause a shift of the G band [21,22]. At excitation wavelengths in the visible range such as 632.8 nm , there is no dependence of the G band position on the sp^3 fraction.

Raman spectroscopy at 632.8 nm excitation wavelength probes the whole bulk of a thin, optically transparent DLC film

(up to some micrometers) and also the substrate. Fig. 1 also shows a contribution from silicon around 1000 cm^{-1} , see also Ref. [23].

The Raman measurements were performed on a Dilor LabRam spectrometer. The excitation light source was a HeNe laser at 632.8 nm with a power of 25 mW . The spectrometer is equipped with two different gratings (600 lines/mm and 1800 lines/mm) and selectable magnification. We used the 1800 lines/mm grating with magnification of 50 for the analysis, as for this configuration the investigated area is comparable to the sensitive area of the other characterization methods ($\leq 1 \text{ mm}^2$) at the highest possible wavenumber resolution. The spectra were fitted with a Breit–Wigner–Fano (BWF) curve to represent the G band, and a Lorentzian (as recommended in e.g. Ref. [24]), to represent the D band. The BWF curve is given as

$$I(\omega) = I_0 \cdot \frac{(1 + 2(\omega - \omega_0)/Q\Gamma)^2}{1 + (2(\omega - \omega_0)/\Gamma)^2}, \quad (3)$$

where ω is the Raman shift, ω_0 the center position, Γ the width parameter and I_0 an amplitude scaling factor. The Q -factor is responsible for the typical asymmetric shape of a BWF curve. A linear background was also included in the fit. The BWF curve was found to be centered in the range of $1565\text{--}1580 \text{ cm}^{-1}$ for all samples. The amplitude of the fitted Lorentzian was found to be very small compared to the amplitude of the G band; $I(D)/I(G)$ was below one percent for all measured samples. All measured samples can therefore be considered to be of good quality in terms of a high sp^3 fraction [19]. The signal-to-background ratio was too low for the samples with film thicknesses below 40 nm , therefore, no Raman results can be given for samples 5, 6 and 8. The lack of a sufficient Raman signal can be used as a first quality control feature. Films with very small or no Raman signal may be too thin for use as wall coating material in UCN applications. As mentioned in the Introduction, wall coatings should be at least 100 nm thick to prevent additional UCN losses due to an insufficiently thick DLC layer.

3.2. X-ray photoelectron spectroscopy

X-ray Photoelectron Spectroscopy (XPS) is one of the standard methods for the determination of the sp^2 and the sp^3 fractions in amorphous carbon films on an absolute level. The chemical bonds of the carbon atoms show up as a composition of slightly different atomic energy levels. The resulting, broadened C1s peak of DLC films thus contains the sp^2 peak at 284.4 eV and the sp^3 peak at 285.2 eV , which can be deconvolved with good resolution [9], as shown in Fig. 2. Typically, there is also a small contribution around 286.5 eV , attributed mainly to C–O bonds at the very surface due to contamination by air exposure, which are potentially also related to some minor contributions from various hydrocarbons. Hydrogen, which is a strong up-scatterer for UCN, is to be kept at a low level in UCN applications. A larger contribution of the 286.5 eV peak can therefore indicate a contamination of the DLC film that would result in an

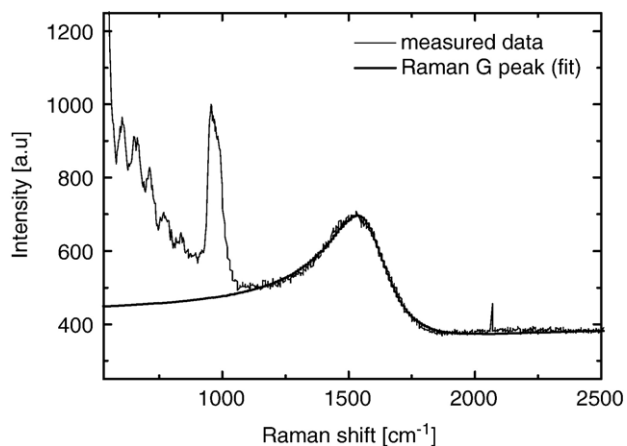


Fig. 1. The original Raman data for the DLC sample 3 (measured with the 600 lines/mm grating), together with the Breit–Wigner–Fano fit for the G band. No significant D band contribution was found. A linear background was included in the fit. The prominent feature around 1000 cm^{-1} comes from the Si substrate.

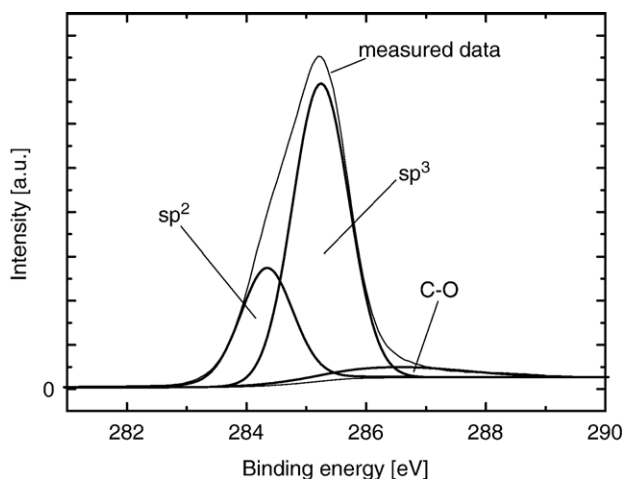


Fig. 2. The XPS spectrum of DLC sample 3, with its decomposition into a Shirley background and the sp^2 (at 284.4 eV), sp^3 (at 285.2 eV) and C–O (at 286.5 eV) peaks.

increased loss probability upon collisions of UCN with the wall material.

The bond fractions are represented by the peak areas. In contrast to other methods, the spectra display only very low background. The determination of the sp^3 fraction is independent of contaminants in the film, to which XPS is very sensitive, as long as their binding energy is not in the range of the C1s peak. In order to find such contamination a XPS survey covering the full energy range up to 1100 eV was performed. No significant contamination was found. Another advantage, particularly for UCN applications, is the fact that the film is probed only to a depth of approximately 3 nm, which is close to the UCN penetration depth upon reflection of about 10 nm. Therefore XPS and UCN probe a similar depth range.

The measurements have been performed on an ESCALAB 220i XL spectrometer using an Al $K\alpha$ monochromatic X-ray source. All samples have been measured as produced, without any special cleaning; only dry air has been used to remove macroscopic dust particles. The pressure in the XPS chamber was below $5 \cdot 10^{-7}$ Pa. The data analysis has been performed with XPSPeak, which is a freely available software package [25]. The peak evaluation followed closely the procedure given in Ref. [9]. After the subtraction of a Shirley background [26], the peaks corresponding to the sp^2 , sp^3 and C–O fraction were fitted with symmetric Gaussian–Lorentzian sum functions [27]. The fit parameters from Ref. [9] were refined by using the spectra from all samples simultaneously: The sp^2 peak is constrained to (284.4 ± 0.1) eV (FWHM= (1.0 ± 0.1) eV), the sp^3 peak to (285.2 ± 0.1) eV (FWHM= (1.1 ± 0.1) eV) and the C–O peak to (286.5 ± 0.2) eV (FWHM= (1.5 ± 1.4) eV). The C–O fraction was found to be proportional to the sp^2 fraction for all measured samples. Therefore the carbon atom in the C–O compound is considered to be sp^2 hybridized. For computing the film density we have therefore assumed the small C–O fraction to have the same density as the purely sp^2 hybridized sections. Then Eq. (2) extends to

$$\rho = a \cdot \rho_3 + (b + c) \cdot \rho_2, \quad a + b + c = 1 \quad (4)$$

where a , b and c are the relative contributions of the sp^3 , sp^2 and C–O peak areas. The results including statistical errors are summarized in Table 2. There is a general decrease in the sp^3 fraction from samples 1 to 4, clearly related to the decreasing sp^3 fraction, as expected from the production process parameters. The sp^2 fraction in contrast is increasing. The relative number of C–O bonds stays on a low level, in between three and seven percent of the total number of carbon bonds. This is in agreement with the findings of other investigations [28] and can be explained by surface contamination, as mentioned above. Subsequent tests have shown that the C–O peak is significantly increased, up to a fraction of 20%, if the DLC is cleaned with e.g. methanol. Based on the process parameters, sample 5 is expected to have about the same film density as sample 1, and sample 6 the same as sample 2, assuming that the film density of the surface layer is independent of the film thickness. Within errors, the XPS results support this. Samples 7 and 8, however, are of low quality in terms of the film density and are therefore not candidates for a high-quality UCN wall coating.

3.3. X-ray absorption near-edge spectroscopy

X-ray Absorption Near-Edge Spectroscopy (XANES), sometimes also called Near-Edge X-ray Absorption Fine-structure Spectroscopy (NEXAFS), is another method that has been widely used for amorphous carbon film characterization for over a decade [29].

The XANES spectrum of DLC consists of a broad feature around 295 eV and a “pre-edge” peak at 285.5 eV, subsequently denoted by $p(sp^2)$, as can be seen in Fig. 3. This first peak in the rising edge of the main feature was identified as a $1s \rightarrow \pi$ transition whereas the main peak (denoted by $p(mf)$) is caused by both $1s \rightarrow \pi$ and $1s \rightarrow \sigma$ transitions [30]. As $p(sp^2)$ is caused by graphitic bonds only it can be used as an indicator for sp^2 sites after proper normalization. We have used this fact to derive a simple phenomenological analysis prescription, using the fact that the XANES spectra for pure graphite (100% sp^2) and pure diamond (0% sp^2) are known and can be used for absolute normalization. We extracted the peak amplitudes of $p(sp^2)$ and $p(mf)$, $A(p(sp^2))$ and $A(p(mf))$, calculated the ratio $A(p(sp^2))/A(p(mf))$ and compared this to the calculated curve obtained from the graphite and diamond reference spectra [31]. This curve was assumed to be a linear function defined by the

Table 2
Results of the XPS measurements

Sample	sp^2 fraction [%]	sp^3 fraction [%]	C–O fraction [%]	Film density [g/cm^3]
1	21.0±0.4	74.0±0.1	4.9±0.5	2.93±0.01
2	28.4±1.0	66.3±0.8	5.3±0.3	2.83±0.01
3	30.5±0.8	64.2±0.8	5.3±0.1	2.80±0.01
4	34.2±1.5	59.6±1.0	6.3±0.6	2.74±0.01
5	22.8±1.7	73.1±1.4	4.2±0.3	2.92±0.02
6	31.7±1.6	62.5±1.3	5.8±1.1	2.78±0.02
7	43.0±1.6	50.4±1.5	6.8±0.2	2.61±0.02
8	40.4±1.6	51.7±1.4	8.0±0.2	2.63±0.02

The density was calculated using Eq. (1).

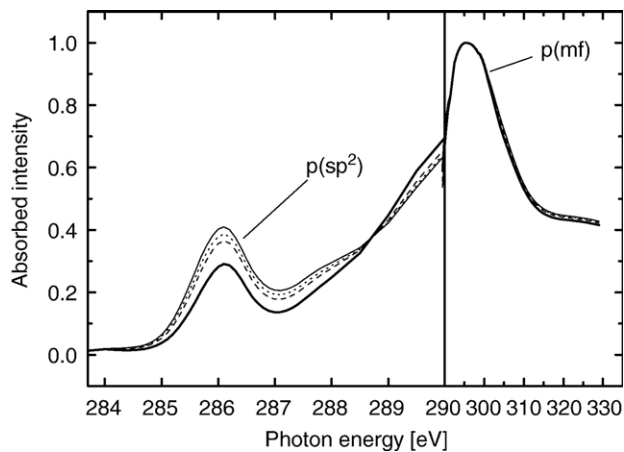


Fig. 3. The XANES spectra of the DLC samples 1–4. The spectra are normalized to a maximum absorbed intensity (at 295 eV) of 1. Please note the change in energy scale at photon energy of 290 eV.

graphite and diamond values for $A(p(sp^2))/A(p(mf))$ and was found to be

$$sp^2 = \frac{A(p(sp^2))}{A(p(mf))} \frac{1}{0.8555} \quad (5)$$

While $A(p(mf))$ is simply the maximum value around 295 eV, the determination of $A(p(sp^2))$ requires the consideration of the background induced by the tail of $p(mf)$. For this, the spectrum was fitted by a sum of Gaussians, following the procedure given in Ref. [31]. In order to account for impurities, which are neither sp^2 nor sp^3 hybridized, but nevertheless contribute to $p(mf)$, the maximum C–O peak contribution determined by XPS was used to enlarge the uncertainties of the sp^3 fraction, calculated as $sp^3 = 1 - sp^2$, to lower values. This leads to asymmetric errors for both the sp^3 fraction and the corresponding film density.

The XANES measurements were performed at the SIM beamline [32] of the Swiss Light Source (SLS). The spectra were acquired in the total electron yield mode measuring the sample photocurrent with an electrometer. The depth sensitivity of XANES is limited by the electron escape depth and is typically around 5 nm. Therefore XANES is similarly sensitive to surface contamination as other X-ray methods like XPS. The results are given in Table 3. The full spectra of samples 1 to 4

Table 3
Results of the XANES measurements

Sample	$A(p(sp^2))/A(p(mf))$	sp^2 fraction [%]	Film density [g/cm^3]
1	0.224 ± 0.017	$26.2^{+8.3}_{-2.0}$	$2.93^{+0.03}_{-0.11}$
2	0.271 ± 0.023	$31.7^{+8.4}_{-2.7}$	$2.86^{+0.04}_{-0.12}$
3	0.301 ± 0.024	$35.1^{+8.5}_{-2.8}$	$2.81^{+0.04}_{-0.12}$
4	0.320 ± 0.025	$37.4^{+8.5}_{-2.9}$	$2.78^{+0.04}_{-0.12}$
5	0.227 ± 0.022	$26.5^{+8.4}_{-2.5}$	$2.93^{+0.04}_{-0.11}$
6	0.271 ± 0.022	$31.7^{+8.4}_{-2.6}$	$2.86^{+0.04}_{-0.12}$
7	0.312 ± 0.020	$36.5^{+8.3}_{-2.4}$	$2.79^{+0.04}_{-0.11}$
8	0.311 ± 0.025	$36.3^{+8.5}_{-2.9}$	$2.79^{+0.04}_{-0.12}$

The sp^2 fraction and the corresponding density were calculated using the values for $A(p(sp^2))/A(p(mf))$ of graphite and diamond.

are shown in Fig. 3. The film density was calculated using Eq. (2) and $sp^3 = 1 - sp^2$. Samples 1 to 4 show clearly a systematic decrease of the sp^3 fraction and of the film density, as expected from the process parameters. As the results for samples 1 and 5 as well as for samples 2 and 6 agree within statistics, it can again be concluded that the density in the surface layer of the film does not depend on how thick the total film is.

3.4. Laser induced surface acoustic waves

Mechanical properties like hardness and Young's modulus are directly related to the density of DLC and their determination can therefore be used to measure the density [33]. Here, Young's modulus was determined by measuring the phase velocity of laser induced surface acoustic waves as a function of the frequency (dispersion curve) [34,35]. Fitting the dispersion curve yields Young's modulus of the film and of the substrate. For DLC, Young's modulus increases with the sp^3 fraction [33,36,37]. Details of this method and its application to amorphous carbon films are given in Refs. [17,35]. On this basis a commercially available device has been developed (LAWave [38]) which was used here. It is equipped with a N₂ Laser at a wavelength of 337.1 nm and a wide-band piezoelectric transducer fixed on the sample surface at a distance of several millimeters from the laser focus.

At film thicknesses below about 200 nm the dispersion curve is close to linear (for homogeneous film density) and allows determination of Young's modulus if the film thickness is known [35]. The latter was determined independently by ellipsometry (see [17]), as mentioned above. From Young's modulus the density of a thin DLC film can then be extracted using an empirical relationship [35]. Fig. 4 shows the dispersion curves for the first six samples. The close-to-ideal linearity indicates that the condition of density homogeneity is nearly fulfilled. Table 4 shows the measured Young's moduli as well as the corresponding film densities and sp^3 fractions (calculated via Eq. (2)). The uncertainties given include statistical errors as well as an estimate of the systematic uncertainties which originate mainly from the thickness measurement (see Table 1). The density and consequently the sp^3 fraction decrease with the

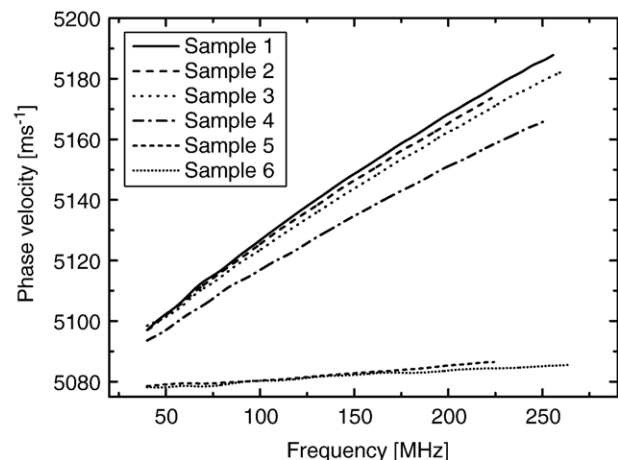


Fig. 4. LAWave frequency spectra for samples 1–6.

Table 4
Results of the LAWave measurements

Sample	Young's modulus (GPa)	Film density [g/cm ³]	sp ³ fraction [%]
1	710±1	3.196±0.004	93.1±0.3
2	633±1	3.083±0.005	84.9±0.4
3	612±1	3.050±0.005	82.5±0.4
4	591±1	3.017±0.003	80.1±0.2
5	543±4	2.936±0.008	74.2±0.6
6	485±4	2.833±0.015	66.6±1.1
7	458±1	2.783±0.015	63.0±1.1
8	358±1	2.583±0.014	48.4±1.0

The film density was calculated using the calibration function published in Ref. [35].

sample number. For samples 1 to 4 this is as expected, i.e. caused by the argon background gas addition. For the thinner films, namely samples 5 and 6, lower densities have been determined. However, as samples 1 and 5 as well as 2 and 6 have been deposited with the same process parameters, the observed difference in the film density of about 0.25 g/cm³ requires explanation (see Section 4).

3.5. Cold neutron reflectometry

As described in the Introduction, neutrons are reflected from certain materials if the velocity component normal to the surface is less than the critical velocity

$$v_c = \sqrt{\frac{2 \cdot V}{m_n}}, \quad (6)$$

V being the Fermi potential and m_n the neutron mass. Cold neutrons with typical velocities of about 500 m/s are thus reflected for angles below about 1° and transmitted for larger angles (see Ref. [39]). The exact determination of the critical reflection angle allows extraction of the Fermi potential and, as a consequence, the density. A distinct advantage of this method for characterization of DLC as wall coating material for UCN applications is that it makes use of neutrons which probe the proper depth range of the samples, around 10 nm. It is therefore a suitable characterization method for UCN wall coatings [39].

Our measurements were performed at the AMOR instrument [40,41] of the Swiss Spallation Neutron Source (SINQ) at PSI. The spectrometer was run in time-of-flight (TOF) mode. This means that the time distribution of the detected neutrons is measured and the velocity obtained from the distance between the TOF chopper and the detector. Fig. 5 shows typical reflectivity spectra as a function of the velocity component normal to the reflection surface. It can be easily seen, e.g. for samples 1 and 7, that the reflectivity decreases rapidly for velocities above about 6.5 m/s, corresponding to a Fermi potential of 220 neV or a film density of 2.55 g/cm³. At a more elaborate level, the reflectivity curve can be predicted by dispersion theory (as originally done for X-rays [42]) and fitted to the measured spectrum in order to extract the film density, thickness and roughness.

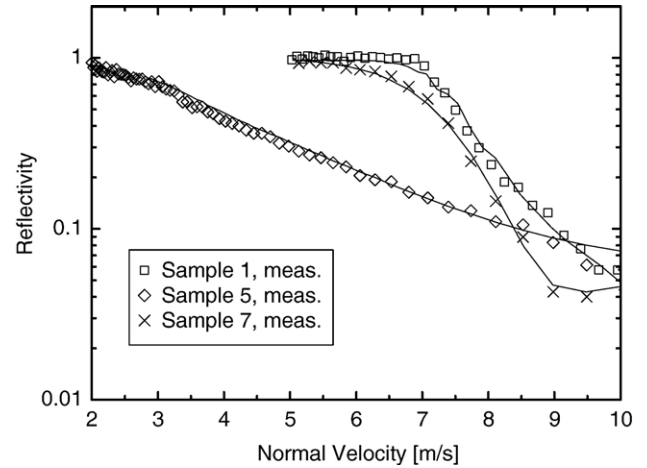


Fig. 5. Neutron reflectivity of selected DLC samples as a function of the normal velocity component. Also included are the calculated fit curves (solid lines).

The reflectivity curves were fitted with the freely available software Parratt32 [43]. A single film layer model was used. The film thickness obtained from optical ellipsometry was used as fixed parameter. Fit parameters were the roughness of both substrate and film and, most importantly, the scattering length density (SLD) of the film. It is the product of the scattering length, which is 6.646 fm for carbon [44], and the particle density (for which diamond has the highest value of all known materials). Therefore from the SLD and knowing the material composition one can derive the particle density and consequently the mass density and the sp³ fraction, respectively. The scattering length values of air and of the silicon substrate were set to literature values [44]. Also the instrument resolution was taken into account. However, the uncertainties of the cold neutron reflectometry measurement depend on the flatness of the investigated samples. Although the silicon wafers used have a small roughness, this does not imply a correspondingly high flatness over the whole coated sample. The unevenness of the sample decreases the resolution of the neutron spectrometer. This leads to increased uncertainties in the fitting process and consequently to large uncertainties in the final results. The measured reflectivity curves, as well as the corresponding fits, are shown in Fig. 5, the results of the curve fitting are summarized in Table 5.

The results for the thicker samples (1 to 4) show a systematic decrease with sample number. The curves of the thinner samples

Table 5
Results of the cold neutron reflectivity measurements

Sample	Scattering length density [Å ⁻¹]	Film density [g/cm ³]	sp ³ fraction [%]
1	(1.03±0.06) · 10 ⁻⁵	3.10±0.17	86±12
2	(1.03±0.06) · 10 ⁻⁵	3.10±0.17	86±12
3	(9.95±0.52) · 10 ⁻⁶	2.99±0.15	78±11
4	(9.56±0.52) · 10 ⁻⁶	2.87±0.16	69±11
5	(9.8±1.1) · 10 ⁻⁶	2.93±0.34	73±25
6	(9.21±0.53) · 10 ⁻⁶	2.76±0.16	62±12
7	(9.23±0.89) · 10 ⁻⁶	2.77±0.27	62±19
8	(8.17±0.86) · 10 ⁻⁶	2.45±0.26	39±19

The film density and the corresponding sp³ fraction were calculated from the particle density which was derived from the scattering length density.

(5, 6 and 8) display an almost exponential behavior over the entire range measured which can only be explained if one assumes that the substrate roughness is of the order of the film thickness. This is the case for the thin samples, as the averaged roughness, R_a , of the silicon substrates was determined independently (with a Perthometer S3P) as close to 10 nm. As the film thickness of sample 7 is somewhere in between that of the first four samples and the thin ones, this sample only shows an increased smoothing around the critical velocity.

4. Discussion

Based on the sub-implantation model for the DLC growth mechanism (see Refs. [45–47]), the results are best discussed by considering the films to have two layers: (i) a carbon bulk layer with homogeneous DLC structure and (ii) a surface layer with probably reduced density, which also contains some contamination (e.g. oxygen, hydrocarbons). From this picture one might expect differences when comparing the results of methods with different depth sensitivity (surface-sensitive XPS and XANES versus bulk-sensitive LAwave and Raman) and samples with various film thicknesses.

The results from the previous section, expressed in terms of density and the corresponding Fermi potential, are summarized in Fig. 6. For further discussion of the results and, particularly, their impact on the desired standard characterization procedure, we split the samples into three groups: (a) samples 1 to 4, with thickness of the order of 100 nm, samples 5,6 and 8, with a thickness in the order of 10 nm, and sample 7 with an intermediate thickness of about 50 nm.

(a) The bulk-sensitive method LAwave shows sp^3 fractions which are up to 20% higher than those obtained by the surface-sensitive methods XPS and XANES. This is to be expected from the sub-implantation model, although the difference is quite large. The results obtained by XPS and XANES are consistent within their uncertainties. The results from cold neutron reflectometry lie in between those of the surface-sensitive methods and the bulk-sensitive methods. Although the uncertainties in cold neutron reflectometry results are large, the method is useful for cross-checking and for obtaining more direct data about the Fermi potential of the DLC coating. From the results of the first four

samples we conclude that the ideal characterization procedure for DLC as wall coating material for UCN application should include a surface-sensitive method, in order to find the minimal density of the coating, i.e. the density of the surface layer. As both, XPS and XANES, probe about the same depth, the method, which determines the sp^3 fraction directly and which has the smaller uncertainties, is to be preferred. This method is XPS.

(b) The results for the thin samples are in reasonable agreement. There is no systematic difference between bulk-sensitive and surface-sensitive methods, also the results of the cold neutron reflectometry are consistent with those of the other methods. This can be easily understood if one considers that for thin coatings one cannot distinguish between surface layer and bulk as they are (nearly) identical. Such a thin coating has about the same density as the surface of a thicker coating would have, if prepared with the same process parameters. Thus, the lower densities obtained by LAwave for samples 5 and 6 compared to samples 1 and 2, which were produced using the same process parameters, are due to the reduced film thickness. Using too thin coatings for UCN applications would result in an increased transmission through the film.

(c) Sample 7 (about 50 nm thick) shows results that lie somewhere in between the 100 nm and the 10 nm thick films. There is a slight difference between surface-sensitive methods and bulk-sensitive methods, however, much smaller than for the thick samples. The difference for the sp^3 fraction is of the order of 10%. Thus, sample 7 does not reveal new information but supports the findings in categories (a) and (b).

5. Conclusions

DLC films with different thicknesses were deposited on silicon wafers using the vacuum arc deposition technique. The sp^3 fraction was varied by adding argon at different partial pressures to the deposition chamber. In order to find an optimal characterization procedure for DLC used as wall coating material in UCN applications, the samples were investigated with fundamentally different methods, namely Raman Spectroscopy, XPS, XANES, LAwave and cold neutron reflectometry.

The sp^3 fraction was extracted directly from XPS and the sp^2 fraction from XANES and XPS, Young's modulus from LAwave and the critical velocity for neutron reflection from cold neutron reflectometry. These parameters were then converted into density by using calibration curves taken from the literature. For film thicknesses around 100 nm the surface-sensitive methods (XPS, XANES) yield lower densities (by up to 20%) compared to the bulk-sensitive LAwave method. This finding is in qualitative agreement with the picture of a thin surface layer (several nm thick) with reduced density residing on a bulk layer with nominal density. The results obtained by cold neutron reflectometry, which is also surface-sensitive, have large uncertainties but are consistent with XPS, XANES and LAwave. For film thicknesses around 10 nm the results of all four methods are consistent and agree with the density obtained by the surface-sensitive methods when applied to thick film samples. This indicates that 10 nm thick DLC films can be considered as being of surface character throughout, with a density similar to that of

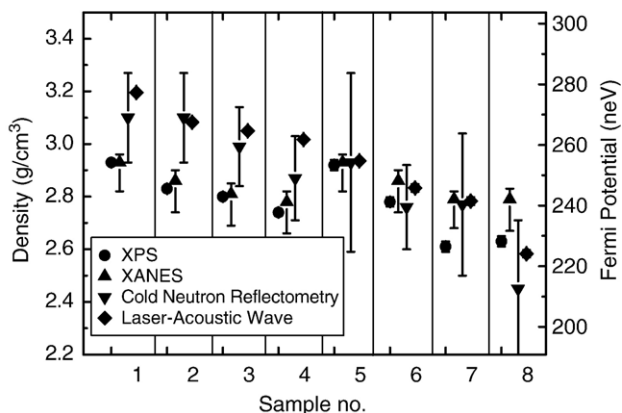


Fig. 6. Results of all characterization methods for all samples.

the surface layer on thick films. The intensity ratio $I(D)/I(G)$ of the two Raman bands was found to be below one percent, indicating an amorphous carbon film with a sp^3 fraction of more than 20%.

In conclusion our results show that the following standard procedure for characterizing DLC coatings as wall coating material in UCN application should be used during production:

- A sample should be quality controlled by Raman spectroscopy. The intensity ratio $I(D)/I(G)$ should be well below 20%. Samples that show no clean Raman signal should not be considered for any further characterization because they are too thin for use as UCN wall coating material.
- Samples should then be investigated with XPS, in order to determine the sp^3 fraction and consequently the density in the uppermost layer. For the use of the DLC film as UCN reflecting material, as in a storage volume or a UCN guide, this information is sufficient.
- If a cross-check of the density is desired, cold neutron reflectometry can be performed on the sample.
- For applications where DLC films are used as transmission filters (e.g. for UCN kinetic energy selection), information about the sp^3 fraction within the bulk of the film is needed. For such applications, the film density can be determined by bulk-sensitive LAwave.

Acknowledgements

This work was performed at the Paul Scherrer Institut, Villigen, Switzerland and at the Fraunhofer Institut für Werkstoff- und Strahltechnik, Dresden, Germany. We appreciate the valuable discussions with J. Berthold, M. Janousch, T. Gutberlet, L. Hardwick, C. Quitmann, L. Patthey, A. Scheidegger and U. Staub. This work is supported by the Swiss National Science Foundation (grant 200021-105400).

References

- [1] V.K. Ignatovich, *The Physics of Ultracold Neutrons*, Oxford University Press, Oxford.
- [2] M. van der Grinten, J. Pendlebury, D. Shiers, C. Baker, K. Green, P. Harris, P. Iaydjiev, S. Ivanov, P. Geltenbort, *Nucl. Instrum. Methods, A* 423 (1999) 421.
- [3] M. Makela, Ph.D. thesis, Virginia Polytechnic Institute and State University, 2005.
- [4] T. Brys, M. Daum, P. Fierlinger, P. Geltenbort, D. George, M. Gupta, R. Henneck, S. Heule, M. Horvat, M. Kasprzak, K. Kirch, K. Kohlik, M. Negrazus, A. Pichlmaier, U. Straumann, V. Vrankovic, C. Wermelinger, *Nucl. Instrum. Methods, A* 550 (2005) 637.
- [5] F. Atchison, T. Brys, M. Daum, P. Geltenbort, R. Henneck, S. Heule, M. Kasprzak, K. Kirch, A. Pichlmaier, C. Plonka, U. Straumann, C. Wermelinger, *Phys. Lett., A* 625 (2005) 19.
- [6] H.-J. Scheibe, B. Schultrich, *Thin Solid Films* 246 (1994) 92.
- [7] E.C. Samano, G. Soto, A. Olivias, L. Cota, *Appl. Surf. Sci.* 202 (2002) 1.
- [8] J. Kulik, Y. Lifshitz, G. Lempert, J. Rabalais, D. Marton, *J. Appl. Phys.* 76 (1994) 5063.
- [9] P. Merel, M. Tabbal, M. Chaker, S. Moisa, J. Margot, *Appl. Surf. Sci.* 136 (1998) 105.
- [10] K. Kanda, Y. Shimizugawa, Y. Haruyama, I. Yamada, S. Matsui, T. Kitagawa, H. Tsubakino, T. Gejo, *Nucl. Instrum. Methods, B* 206 (2003) 880.
- [11] A.C. Ferrari, J. Robertson, *Phys. Rev., B* 61 (2000) 14095.
- [12] D. Knight, W. White, *J. Mater. Res.* 4 (1989) 385.
- [13] M. Guerino, M. Massi, H.S. Maciel, C. Otani, R.D. Mansano, P. Verdonck, J. Libardi, *Diamond Relat. Mater.* 13 (2004) 316.
- [14] M. Pandey, D. Bhattacharyya, D.S. Patil, K. Ramachandran, N. Vekratmani, *Surf. Coat. Technol.* 182 (2004) 24.
- [15] B. Petereit, P. Siemroth, H.-H. Schneider, H. Hilgers, *Surf. Coat. Technol.* 174–175 (2003) 648.
- [16] B. Schultrich, C.-F. Meyer, H.-J. Scheibe, T. Witke, H. Ziegele, *Mat. Sci. Forum* 287–288 (1998) 381.
- [17] D. Schneider, P. Siemroth, T. Schülke, J. Berthold, B. Schultrich, H.-H. Schneider, R. Ohr, B. Petereit, H. Hilgers, *Surf. Coat. Technol.* 153 (2002) 252.
- [18] A.C. Ferrari, A. Libassi, B.K. Tanner, V. Stolojan, J. Yuan, L.M. Brown, S.E. Rodil, B. Kleinsorge, J. Robertson, *Phys. Rev., B* 62 (2000) 11089.
- [19] A.C. Ferrari, J. Robertson, *Phys. Rev., B* 64 (2001) 075414.
- [20] S. Sails, D. Gardiner, M. Bowden, J. Savage, D. Rodway, *Diamond Relat. Mater.* 5 (1996) 589.
- [21] J. Ager, S. Anders, A. Anders, I. Brown, *Appl. Phys. Lett.* 66 (1995) 3444.
- [22] J. Schwan, S. Ulrich, V. Batori, H. Ehrhardt, S.R.P. Silva, *J. Appl. Phys.* 80 (1996) 440.
- [23] P.A. Temple, C.E. Hathaway, *Phys. Rev., B* 7 (1973) 3685.
- [24] S. Praver, K.W. Nugent, Y. Lifshitz, G.D. Lempert, E. Grossman, J. Kulik, I. Avigal, R. Kalish, *Diamond Relat. Mater.* 5 (1996) 433.
- [25] XPSPeak, written by R. Kwok, download at <http://www.phy.cuhk.edu.hk/~surface/XPSPEAK/>.
- [26] D. Shirley, *Phys. Rev., B* 5 (1972) 4709.
- [27] G. Wertheim, M. Butler, K. West, D. Buchanan, *Rev. Sci. Instrum.* 45 (1974) 1369.
- [28] J.C. Lascovich, R. Giorgi, S. Scaglione, *Appl. Surf. Sci.* 47 (1991) 17.
- [29] G. Comelli, J. Stöhr, W. Jark, *Phys. Rev., B* 37 (1988) 4383.
- [30] T. Capehart, T. Perry, C. Beetz, D. Belton, G. Fisher, C. Beall, B. Yates, J. Taylor, *Appl. Phys. Lett.* 55 (1989) 957.
- [31] J. Stöhr, *NEXAFS Spectroscopy*, Springer, 1992.
- [32] C. Quitmann, U. Flechsig, L. Patthey, T. Schmidt, G. Ingold, M. Howells, M. Janousch, R. Abela, *Surf. Sci.* 480 (2001) 173.
- [33] J. Robertson, *Surf. Coat. Technol.* 50 (1991) 185.
- [34] D. Schneider, H.-J. Scheibe, T. Schwarz, P. Hess, *Diamond Relat. Mater.* 2 (1993) 1396.
- [35] D. Schneider, T. Schwarz, H.-J. Scheibe, M. Panzner, *Thin Solid Films* 295 (1997) 107.
- [36] Y. Lifshitz, *Diamond Relat. Mater.* 8 (1999) 1659.
- [37] D. Schneider, C.F. Meyer, H. Mai, B. Schöneich, H. Ziegele, H.J. Scheibe, Y. Lifshitz, *Diamond Relat. Mater.* 7 (1998) 973.
- [38] Fraunhofer Institut für Werkstoff- und Strahltechnik, Dresden <http://www.iws.fhg.de>.
- [39] E. Feidenhans'l, M.E. Vigild, K.N. Clausen, J. Bindslev Hansen, M.D. Bentzon, J.P. Goff, *J. Appl. Phys.* 76 (1994) 4636.
- [40] D. Clemens, P. Gross, P. Keller, N. Schlumpf, M. Könnecke, *Physica B* 276–278 (2002) 140.
- [41] M. Gupta, T. Gutberlet, J. Stahn, P. Keller, D. Clemens, *Pramana — J. Phys.* 63 (2004) 57.
- [42] L. Parratt, *Phys. Rev.* 95 (1954) 359.
- [43] Parratt32, written at HMI Berlin, download at http://www.hmi.de/bensch/instrumentation/instrumente/v6/refl/parratt_en.htm.
- [44] V. Sears, *Neutron News* 3, vol. 3, 1992, p. 29ff.
- [45] J. Robertson, *Diamond Relat. Mater.* 2 (1993) 984.
- [46] J. Robertson, *Diamond Relat. Mater.* 3 (1994) 361.
- [47] J. Robertson, *Diamond Relat. Mater.* 14 (2005) 942.